Analysis of the nonlinear dynamics of a 2–axle freight wagon in curves

Egidio Di Gialleonardo[a]*, Stefano Bruni[a] and Hans True[b]

[a]*Dipartimento di Meccanica, Politecnico di Milano,Via La Masa 1, I-20156 Milan, Italy;* [b]*DTU Compute, Technical University of Denmark, Matematiktorvet 303B, DK-2800 Kgs, Lyngby, Denmark*

(*Received 4 July 2013; accepted 3 November 2013*)

1. Introduction

Rail transport is among the most energy-efficient means to displace freights over a wide range of distances. However, the increased competition from air and road transport requires that the speed and capacity of freight transport on railway lines is continuously improved. This is being achieved by increasing the total hauled mass (super long freight trains) and by raising the speed of the wagons. Both options are posing serious problems to railway engineers and specifically to railway dynamicists: for very long trains, braking and tractive forces and their effect on lateral dynamics (e.g. while negotiating a curve) are an issue, whereas the increase in the vehicle speed requires that the possible onset of hunting motion is carefully considered: this is the issue dealt with by this paper.

Railway freight wagons represent highly nonlinear and nonsmooth systems due to the nonlinearities related with wheel–rail contact and to the fact that energy dissipation in the suspensions is obtained by means of dry friction elements. Therefore, the analysis of their running behaviour needs to be performed using appropriate models for dry friction suspension elements [1] and suitable techniques to investigate the existence of periodic solutions and

*Corresponding author. Email:
egidio.digialleonardo@polimi.it

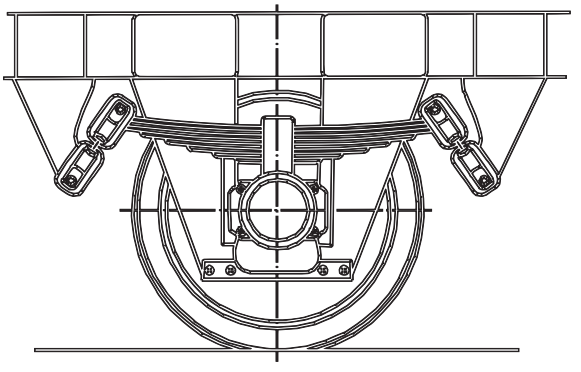

Figure 1. Standard UIC suspension.

analyse bifurcations in nonsmooth systems,[2–5] thereby determining the correct critical speed of the vehicle.[6]

From the point of view of modelling nonsmoothness in the suspension, this paper focuses on 2-axle wagons featuring the standard Union internationale des chemins de fer (UIC) suspension (Figure 1), composed by a leaf spring and a system of links called UIC links. Fancher et al. [7] provided a comprehensive mathematical model to represent the nonlinear displacement-force characteristics and the friction damping effects in leaf springs. Further details on the modelling of leaf springs can be found in the book by Cebon.[8]

As far as the modelling of the UIC links is concerned, Piotrowski [9] developed a mathematical model taking into account the nonsmooth rolling/sliding transitions taking place in the links during operation and derived the model parameter values from theoretical considerations assuming a nominal geometry of the links. Piotrowski also proposed a method to measure the mechanical characteristics of the UIC link suspension from tests performed on the component.[10] The influence of wear in the link elements was investigated by Grzelak [11] and Jönsson.[12] The latter found in his measurements that the rolling stiffness normally increases with wear and that new links often exhibit a very low amount of energy dissipation.

With regard to the dynamics of a 2-axle freight wagon, Stichel suggested the possible occurrence of a resonance between the kinematic hunting of the wheelsets and the yaw eigenmode of the carbody.[13] He also observed that the lateral motion of 2-axle wagons might settle into an attractor whose structure is broadband [14] and that on account of their structural flexibility open-sided wagons may have modes of vibration associated with carbody flexibility in the frequency range below 10 Hz which may affect their running behaviour.[15] Hoffmann in his thesis [16] provided a comprehensive investigation of the nonlinear dynamics of a 2-axle freight wagon in straight track, showing that rail inclination has an important influence on the wagon running behaviour and proving the possibility of the resonance between Klingel motion and the yaw eigenmode of the carbody. He recognised, however, the need for further research to be performed to analyse the behaviour of this vehicle in a curve.

Aim of this work is therefore to study the nonlinear dynamics of the single 2-axle freight wagon in a curve, defining the stationary periodic solutions and the bifurcation diagrams as function of the running conditions of the vehicle (curve radius and speed). The paper also aims at analysing the case of an assembly of wagons negotiating a curve, taking into account the forces exchanged through the buffers and the draw gear.

To this end, a multi-body model is introduced for a single 2-axle wagon in a curve, including the nonlinear/nonsmooth description of the behaviour of the UIC standard suspensions and the

nonlinear/nonsmooth aspects of wheel–rail contact. The model is then extended to represent an assembly of three wagons. In both cases (single wagon and car assembly), a numerical analysis of the steady-state solution reached after the negotiation of curve transition is presented and bifurcations are identified for some particular values of the curve radius by means of the ramping method.[17]

The paper is organised as follows: in Section 2, the multi-body model of the single wagon is presented, paying particular attention to the nonlinear/nonsmooth modelling of the suspensions. In Section 3, the model of the inter-car forces generated by the buffers and chain coupling system is introduced. Sections 4 and 5 present the results obtained for the single wagon and car assembly, respectively. Finally, Section 6 provides some conclusive remarks.

2. Mathematical model of the single wagon

The multibody model was defined using program ADTreS, an in-house software for the numerical simulation of rail vehicle dynamics and train track interaction developed at Politecnico di Milano, Department of Mechanical Engineering. The single wagon model includes three bodies: the carbody and two wheelsets. Since the study is confined to the low-frequency dynamics of the vehicles (below 20 Hz), both the carbody and the wheelsets are assumed to behave as rigid bodies. For the same reason, the effect of track flexibility is neglected in this study.

The motion of the wagon is described with respect to a moving Cartesian reference travelling with constant speed V along the track centreline and keeping the Z axis tangent to the track centreline and the X axis orthogonal to the rail level. The motion of the moving reference can be defined in terms of the time histories of two successive rotations $\theta_X(t)$ and $\theta_Z(t)$ around the X and Z axes which can be expressed 'a priori' as function of track geometry and of the vehicle forward speed V.

The forward movement of all bodies is assumed to take place with constant speed V, so that for each kth rigid body 5 independent coordinates are introduced, consisting of the displacements x_k and y_k along the X and Y directions of the moving reference and of the three rotations σ_k (yaw), β_k (pitch) and ρ_k (roll) around the X, Y and Z axes, respectively, and resulting in a total of 15 independent kinematic coordinates for one wagon. The motion of each body is assumed to represent a small perturbation with respect to the motion of the moving reference (except for the pitch rotation β_k of the two wheelsets, which is assumed to be a small perturbation with respect to the constant rolling speed), so that nonlinear terms in the equations of motion associated with the large rigid body motion are avoided.

2.1. *The model of vehicle suspensions*

The 2-axle freight wagons considered in this study are equipped with the UIC standard suspension, as shown in Figure 1. The suspension includes two main components: the leaf spring and the double-link. The leaf spring is used as a vertical suspension, and also provides energy dissipation through the dry friction forces generated at the interface between the leaves. The double-link acts as a pendular suspension system in the horizontal plane, yielding stiffness in both lateral and longitudinal directions. Dry friction is also introduced in the joints of the link, providing the necessary damping for the horizontal motion. The axle guidance system, see Figure 1, provides further restraint of the axle box with respect to the carbody, in the form of a large stiffness with clearance.

2.1.1. *The leaf spring model*

The mathematical model of the leaf spring used in this work is the one presented by Hoffman in [16], based on the work by Fancher et al. [7] and Cebon,[8] which can be adapted to represent both trapezoidal and two-stage parabolic leaf spring types. The restoring force from the leaf spring is expressed by the following differential equation:

$$\dot{F}_{\mathrm{LS}} = \frac{F_{\mathrm{env}} - F_{\mathrm{LS}}}{\alpha} |\Delta \dot{l}_x|, \tag{1}$$

where F_{LS} is the restoring force from the leaf spring, F_{env} is an envelope function, $\Delta \dot{l}_x$ is the relative velocity between the attachment points of the leaf spring on the carbody and on the axle and α is a decay constant. The envelope function defines the upper and lower boundaries of the hysteresis loop generated by the model, whereas the decay constant determines how steep the transition between the two boundaries should be.

The envelope function F_{env} is defined as follows:

$$F_{\mathrm{env}} = \begin{cases} c_h(1+\mu_0)\Delta l_x + F_{\mathrm{r}} & \Delta l_x < \Delta l_0, \Delta \dot{l}_x > 0 \quad \text{(loading)}, \\ c_x(1+\mu_0)(\Delta l_x - \Delta l_*) + F_{\mathrm{r}} & \Delta l_x > \Delta l_0, \Delta \dot{l}_x > 0 \quad \text{(loading)}, \\ c_h(1-\mu_0)\Delta l_x - F_{\mathrm{r}} & \Delta l_x < \Delta l_0, \Delta \dot{l}_x < 0 \quad \text{(unloading)}, \\ c_x(1-\mu_0)(\Delta l_x - \Delta l_*) - F_{\mathrm{r}} & \Delta l_x > \Delta l_0, \Delta \dot{l}_x < 0 \quad \text{(unloading)}, \end{cases} \tag{2}$$

where c_h is the spring stiffness with an inactive additional leaf, c_x is the spring stiffness with an active additional leaf, μ_0 is a friction parameter, $\Delta l_\times$ is the deformation of the spring, Δl_0 is the position of the additional leaf and F_{r} is the residual spring force. For two-stage leaf springs Δl_0 assumes a finite value whereas for one-stage leaf springs $\Delta l_0 = \infty$. The constant parameter Δl_* in Equation (2) is defined as

$$\Delta l_* = \begin{cases} \left(1 - \frac{c_h}{c_x}\right) \Delta l_0 & 0 < \Delta l_0 < \infty, \\ 0 & \Delta l_0 = \infty. \end{cases} \tag{3}$$

Equations (1)–(3) provide altogether a nonlinear differential description of the restoring force in the leaf spring, involving one internal state variable.

2.1.2. *The UIC double-link model*

The second element composing the UIC standard suspension is the double-link connecting the leaf spring and the carbody, see Figure 2, left. This device is composed by two pins, four end bearings which may roll over the pins, four links mounted on the end bearings with a possibility to roll in a direction orthogonal to the pins and by an intermediate bearing coupling the two single link systems.

This component can be seen as a combination of technical pendulums,[9] the single technical pendulum being different from an idealised mathematical pendulum in that rolling and sliding in the joints are taken into account. In the lateral direction, the deformation of the suspension is due to the roll of the links over the end bearings, whereas in the longitudinal direction it is due to the roll of the end bearings over the pins. An important feature of this suspension component is that the design of the end bearing allows to consider the lateral and the longitudinal dynamics of the double-link connection as completely uncoupled. In both directions, a restoring force is generated by the increase in the gravitational potential energy entailed by a displacement of the axle box relative to the carbody, like in an ordinary pendulum, whereas damping comes

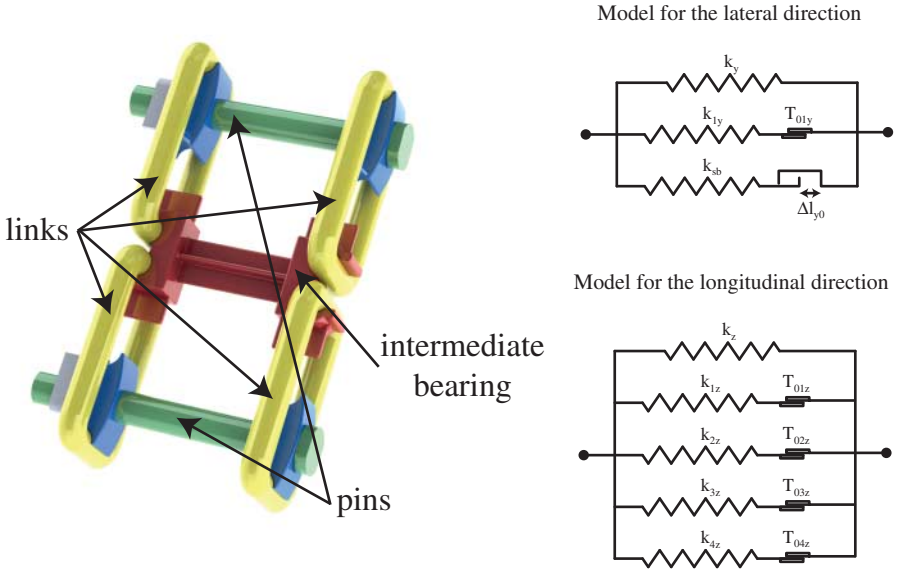

Figure 2. Left: the UIC double-link. Right: model of the UIC link by Piotrowski [9].

from dry friction in the joints. However, energy dissipation is only present when the amplitude of the excitation exceeds a certain threshold, since for small amplitude movements the joints experience pure rolling. The critical value of the amplitude of motion corresponding to the transition from pure rolling to sliding depends on many factors, such as the dimensions of the joints, the friction coefficient, the state of wear and so on.

The mathematical model of the UIC double-link used in this paper is due to Piotrowski,[9] see Figure 2, right. In the lateral direction, the model is defined by a linear spring in parallel to an elastic element with dry friction. Another spring with a dead band is included to represent the interaction with the suspension bracket. In the longitudinal direction, the model consists of a linear spring in parallel to several elastic elements with dry friction which are assumed to follow Coulomb's friction law.

The model for the lateral direction is expressed by the following equations:

$$\begin{aligned} F_y(\Delta l_y) &= -k_y \Delta l_y + T_{1y} + F_{sb}, \\ \dot{T}_{1y}(\Delta l_y) &= \begin{cases} -k_{1y}\Delta \dot{l}_y & \text{stick}, \\ 0 & \text{slip}, \end{cases} \\ F_{sb}(\Delta l_y) &= \begin{cases} 0 & \text{idle}, \\ -k_{sb}(\Delta l_y - \Delta l_{y0}) & \text{active side 1}, \\ -k_{sb}(\Delta l_y + \Delta l_{y0}) & \text{active side 2}. \end{cases} \end{aligned} \tag{4}$$

For the longitudinal direction, the equations of the UIC double-link model take the form

$$\begin{aligned} F_z(\Delta l_z) &= -k_z \Delta l_z + \sum_{i=1}^{4} T_{iz}, \\ \dot{T}_{iz}(\Delta l_z) &= \begin{cases} -k_{iz}\Delta \dot{l}_z & \text{stick}, \\ 0 & \text{slip}. \end{cases} \end{aligned} \tag{5}$$

Table 1. Parameters of the UIC link model (normalised with respect to the vertical load applied on the suspension).

	k (1/m)	k_1 (1/m)	k_2 (1/m)	k_3 (1/m)	k_4 (1/m)
Normalised stiffness parameters					
Y	3.41	10.38			
Z	5.51	3.56	1.90	0.35	1.86
	T_{01} (–)	T_{02} (–)	T_{03} (–)	T_{04} (–)	
Normalised friction parameters					
Y	0.05300				
Z	0.02103	0.01425	0.00278	0.02059	

The parameters of the models are defined according to the method proposed by Piotrowski [9] and are reported in Table 1 and it is shown by Mark Hoffman in [16] that they are suitable for reproducing the measured behaviour of the UIC double-link suspension. The parameter k_{sb} is set to the same value of k_{1y} so that the pendulum stiffness is doubled when the clearance between the UIC double-link and the suspension bracket is exceeded. The dry friction coefficient is set to 0.3.

2.2. *Wheel–rail contact model*

The wheel–rail contact model used in this work is based on a multi-Hertzian approach and allows to consider the simultaneous presence of multiple contact points in the same wheel–rail couple.[18,19] Since this research deals with vehicle dynamics along a curved track, the contact model considers the so-called out-of-plane effect, i.e. the fact that, depending on the angle of attack of the wheelset on the track, the contact points lie outside the vertical meridian plane of the wheelset. This effect can be especially important for 2-axle freight cars while negotiating small–medium radius curves, because of the large wheelbase of the two wheelsets which will produce a relatively large angle of attack. To properly consider this effect, the 'visible profile' method [20] is used in this work.

To improve computational efficiency, the contact parameters are stored in a multiple contact table and retrieved by interpolation to compute wheel–rail contact forces in the numerical simulation procedure. The contact table typically contains discontinuities associated with some positions of the wheelset over the track at which small variations of the relative wheelset–track displacement will produce relatively large variations of the contact point position and thereby of the contact parameters. The locations at which discontinuities and/or multiple contacts take place depend on the shape of the wheel and rail profiles: in this study the ORE S1002 wheel profile and the UIC60 rail profile with inclination 1:20 are considered. Full details on the contact model and its validation can be found in [19].

3. Model of the buffer and chain coupling system

When a composition of wagons is considered, the forces exchanged by the wagons through the buffers and chain coupling system need to be modelled. In this work, a mathematical model expressing the forces generated in the buffers and hooks as function of the relative motion of the carbodies is introduced based on references [21,22]. The forces generated at the couplers and buffers as the result of the longitudinal dynamics of the train set are neglected, so the analysis should be regarded as representative of the case of a train running through a curve

in a traction condition close to coasting. If otherwise curving is combined with braking, large traction or compression forces are generated at the couplers and buffers on account of the longitudinal dynamics and of the braking circuit dynamics, which may severely affect the running dynamics of the train set, see [21,23,24].

3.1. *Buffer kinematics*

To describe the dynamic behaviour of the buffers, two additional independent coordinates are introduced for the ith vehicle $\xi_{i,j}$ describing the elongation of the left and right rear buffers with $j = 1$ for the left side and $j = 2$ for the right side. The displacements of the left and right front buffers in the $(i + 1)$th vehicle are denoted by $\eta_{i+1,j}$ and are derived as function of the coordinates of the system considering that the distance between the geometrical centres of two contacting buffer heads equals two times the radius R_1 of the buffer head, cf. Figure 3 (the value $R_1 = 2.75$ m is assumed).

Buffer kinematics is solved below for the left buffer (cf. Figure 3), the same equations hold for the right one. First, the positions of the reference points A_i and D_{i+1} shown in Figure 3 are expressed in the absolute reference system $(\bar{O}, \bar{X}, \bar{Y}, \bar{Z})$ based on the independent coordinates of the vehicles, and the components $z_{i,j}$ and $y_{i,j}$ of the distance between the two points are derived.

On account of the geometry of the buffers, the following system of equations is written:

$$\begin{aligned} z_{i,j} &= \xi_{i,j} \cos\,\theta_i + 2R_1 \cos\,\alpha + \eta_{i+1,j} \cos\,\theta_{i+1}, \\ y_{i,j} &= \xi_{i,j} \sin\,\theta_i + 2R_1 \sin\,\alpha + \eta_{i+1,j} \sin\,\theta_{i+1}. \end{aligned} \tag{6}$$

Manipulating Equation (6), it is possible to obtain an algebraic second-order equation in the unknown $\eta_{i+1,j}$

$$\eta_{i+1,j}^2 + A\eta_{i+1,j} + B = 0, \tag{7}$$

where

$$\begin{aligned} A &= 2\xi_{i,j} \cos\,\theta_i \cos\,\theta_{i+1} + 2\xi_{i,j} \sin\,\theta_i \sin\,\theta_{i+1} - 2\,\cos\,\theta_{i+1} z_{i,j} - 2\,\sin\,\theta_{i+1} y_{i,j}, \\ B &= \xi_{i,j}^2 - 2R_1^2 + z_{i,j}^2 + y_{i,j}^2. \end{aligned} \tag{8}$$

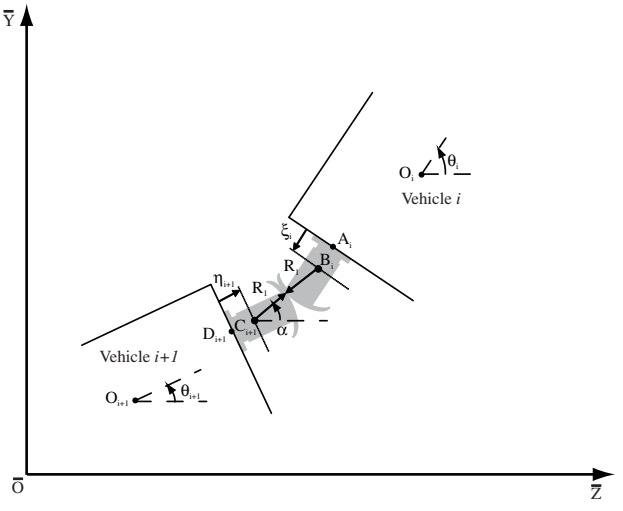

Figure 3. Kinematics of contacting buffers (left buffer).

Equation (7) can be solved for the value of $\eta_{i+1,j}$, in case no real solution is obtained, the two buffers are not in contact, and the transmitted force is set to zero. Otherwise, the speed of deformation and then the transmitted force are computed.

Differentiating Equation (6) with respect to time, it is possible to write

$$2\eta_{i+1,j}\dot{\eta}_{i+1,j} + \dot{A}\eta_{i+1,j} + A\dot{\eta}_{i+1,j} + \dot{B} = 0. \tag{9}$$

It follows that

$$\dot{\eta}_{i+1,j} = -\frac{\dot{A}\eta_{i+1,j} + \dot{B}}{(2\eta_{i+1,j} + A)}. \tag{10}$$

Equations (7) and (10) express both the displacement of each front buffer of the $(i+1)$th vehicle $\eta_{i+1,j}$ and its time derivative $\dot{\eta}_{i+1,j}$ in function of the chosen degree of freedom $\xi_{i,j}$ and its time derivative $\dot{\xi}_{i,j}$.

3.2. *Forces in the buffers*

The axial force generated by the single buffer is defined as function of the elongation and rate of elongation of the buffer $\xi_{i,j}$ and $\dot{\xi}_{i,j}$ (for a rear buffer) or $\eta_{i+1,j}$ and $\dot{\eta}_{i+1,j}$ (for a front buffer). To this end, the model defined by Cheli and Melzi [22] and consisting of a nonlinear spring-damper element is adopted here, thereby expressing the buffer force as a polynomial function of the deformation and of the rate of deformation in the buffer

$$\begin{aligned} F_{n_{i,j}} &= (k_0 + k_1\xi_{i,j} + k_2\xi_{i,j}^2 + k_3\xi_{i,j}^3 + k_4\xi_{i,j}^4)\xi_{i,j} + (r_0 + r_1\xi_{i,j})\dot{\xi}_{i,j}, \\ F_{n_{i+1,j}} &= (k_0 + k_1\eta_{i+1,j} + k_2\eta_{i+1,j}^2 + k_3\eta_{i+1,j}^3 + k_4\eta_{i+1,j}^4)\eta_{i+1,j} + (r_0 + r_1\eta_{i+1,j})\dot{\eta}_{i+1,j}. \end{aligned} \tag{11}$$

In [22], the simple nonlinear model expressed by Equation (11) is compared with a more detailed rheological model and it is concluded that the difference between the two models is negligible when curve negotiation is considered, provided that the traction/braking forces transmitted through the coupling system are small, which is the case considered in this paper, since curving dynamics at constant speed is considered.

The transversal component $F_{t_{i,j}}$ of the force exchanged through the buffers is defined using a smoothed formulation of Coulomb friction.

3.3. *State equations of the buffers*

In order to derive the value of the buffer state variable and its time derivative $\dot{\xi}_{i,j}$ the third Newton's law is applied, imposing that the resultant force on the buffer of the ith vehicle $F_{r_{i,j}}$ is equal and opposite to the force on the buffer of the $(i+1)$th vehicle $F_{r_{i+1,j}}$. It is possible to calculate the resultant force on the buffer once the axial and the transversal component are known:

$$\begin{aligned} F_{r_{i,j}} &= \sqrt{F_{n_{i,j}} + F_{t_{i,j}}}, \\ F_{r_{i+1,j}} &= \sqrt{F_{n_{i+1,j}} + F_{t_{i+1,j}}}. \end{aligned} \tag{12}$$

Writing the functional dependencies on the buffer displacements and their time derivatives, the following relationships are found:

$$\begin{aligned} F_{r_{i,j}} &= f(\xi_{i,j}, \dot{\xi}_{i,j}), \\ F_{r_{i+1,j}} &= f(\eta_{i+1,j}(\xi_{i,j}), \dot{\eta}_{i+1,j}(\xi_{i,j}, \dot{\xi}_{i,j})). \end{aligned} \tag{13}$$

Applying Newton's third law a first-order nonlinear differential equation in the degree of freedom $\xi_{i,j}$ and its time derivative $\dot{\xi}_{i,j}$ is found:

$$f(\xi_{i,j}, \dot{\xi}_{i,j}) - f(\eta_{i+1,j}(\xi_{i,j}), \dot{\eta}_{i+1,j}(\xi_{i,j}, \dot{\xi}_{i,j})) = 0. \tag{14}$$

One state equation in the form (14) is introduced for each couple of buffers in contact in the wagon assembly considered. These equations are numerically integrated together with the equations of motion of the vehicles.

3.4. *Model of the traction gear*

The traction gear considered in this work is made of two hooks and one chain. The dynamical behaviour of this component is reproduced by means of the nonlinear model proposed in [25], also consisting of a nonlinear spring-damper

$$F_g = (k_0 + k_1 \Delta l_g + k_2 \Delta l_g^2 + k_3 \Delta l_g^3 + k_4 \Delta l_g^4) \Delta l_g + (r_0 + r_1 \Delta l_g) \Delta \dot{l}_g. \tag{15}$$

The elongation of the traction gear Δl_g and the rate of deformation $\Delta \dot{l}_g$ are derived from the independent coordinates of the two adjacent wagons using a procedure similar to the one described in Section 3.1 for the buffers.

4. Results for a single wagon

The nonlinear dynamics of the 2-axle wagon in tangent track has been extensively studied in [16]. Aim of this section is to investigate the same problem for a single wagon in a curve, looking for periodic solutions caused by hunting. In principle, solutions should be sought for in a space of codimension-3, defined by three independent parameters: vehicle speed, curve radius and track cant. In order to reduce the dimension of the problem, the study is performed for a fixed value of the track cant in full curve, corresponding to 150 mm super-elevation of the outer rail. In this way, vehicle speed V and full curve radius R become the only two independent parameters of the problem.

The existence of stationary solutions is studied using a twofold approach: first, time domain simulations are performed considering the wagon to travel from an initial tangent track stretch into a curve transition and then into a full curve, for different combinations of parameters V and R; in order to find the steady-state solutions, neither track irregularity nor wheel out-of-roundness are introduced in the simulation. In this way, a map is derived for the existence and amplitude of stationary periodic solutions. However, the nature of the attractors found cannot be completely defined by this analysis, as the solutions found may be affected by perturbations. Therefore, for some representative values of the curve radius, the ramping method [17] is used to identify the bifurcation type and to obtain an estimate of the vehicle speed corresponding to the bifurcation point.

Given that the hunting motion consists of a coupled lateral and yaw oscillation of the vehicle, in this paper the amplitude of the lateral motion A_{y_i} of each ith body (carbody, leading wheelset and trailing wheelset) is used to characterise the solutions of the nonlinear problem. This is defined as one half of the peak-to-peak amplitude of the oscillation

$$A_{y_i} = \frac{\max(y_i) - \min(y_i)}{2} \tag{16}$$

y_i being the lateral displacement of the ith body. Therefore, if the steady-state solution is stationary, A_{y_i} is equal to zero, whereas if it is simple periodic A_{y_i} is the amplitude of the oscillation.

In the first analysis (mapping of the stationary solutions), the curve radius value R is varied step-wise from 250 to 2000 m with 50 m step size. For each curve radius, simulations are performed considering different vehicle speeds, the minimum one corresponding to $-0.8\,\mathrm{m/s^2}$ non-compensated lateral acceleration (n.c.l.a.) and the maximum one corresponding to $0.8\,\mathrm{m/s^2}$ n.c.l.a.

The results presented hereafter refer to a wagon-type Hbbills 311, which is a wagon equipped with sliding sidewalls. For the sake of brevity, only the tare condition configuration is considered in this paper. The main parameters for the wagon are reported in Table 2. ORE S1002 wheel profiles and UIC60 rail profile inclined in 1:20 are considered in all simulations.

Figure 4 shows the oscillation amplitude A_{y_i} as function of the vehicle speed for different curve radii. The three sub-plots show, from top to bottom, the results for the carbody, leading wheelset and trailing wheelset. The largest oscillation amplitudes are observed for the carbody and for the trailing wheelset, whereas the leading wheelset shows oscillation amplitudes close to zero, especially for small radius curves ($R < 1000$ m). This happens because the outer wheel in the leading wheelset is in flange contact with the rail: this contact condition acts as a restraint to the lateral oscillation of the wheelset, which is equal or close to zero.

As far as the carbody and trailing wheelset are concerned, for small radius curves ($R \leq 750$ m) the oscillation amplitude is generally increasing with the speed. On the other hand, for curve radii above 1000 m the maximum oscillation amplitude is obtained for an intermediate speed value, which is increasing with the curve radius and, for the largest radii considered, probably falls outside the maximum service speed of the wagon.

Table 2. Mass and geometric properties of wagons type Hbbills 311 in tare condition.

Wheelset mass (kg)	1490	Carbody mass (kg)	15,176
Wheelset roll moment of inertia (kgm^2)	988	Carbody roll moment of inertia (kgm^2)	32,675
Wheelset pitch moment of inertia (kgm^2)	89.9	Carbody pitch moment of inertia (kgm^2)	422,084
Wheelset yaw moment of inertia (kgm^2)	988	Carbody yaw moment of inertia (kgm^2)	413,250
Wheelbase (m)	10	Carbody c.o.g height above the t.o.r. (m)	1.565
Nominal wheel radius	0.46		

Note: c.o.g., centre of gravity; t.o.r., top of rail.

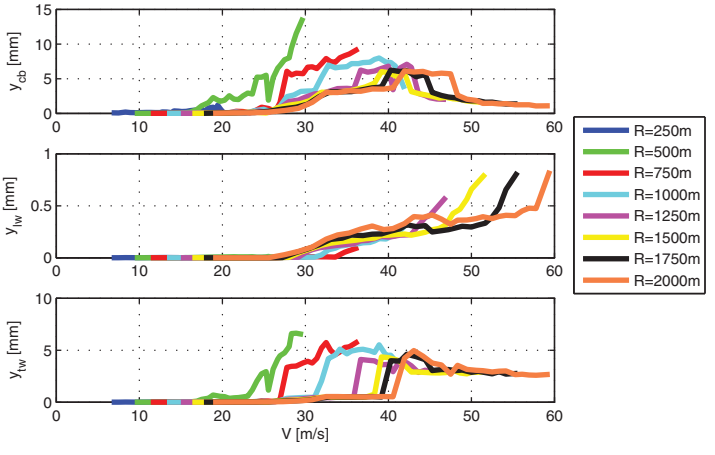

Figure 4. Analysis of the single wagon. Map of the lateral oscillation amplitude.

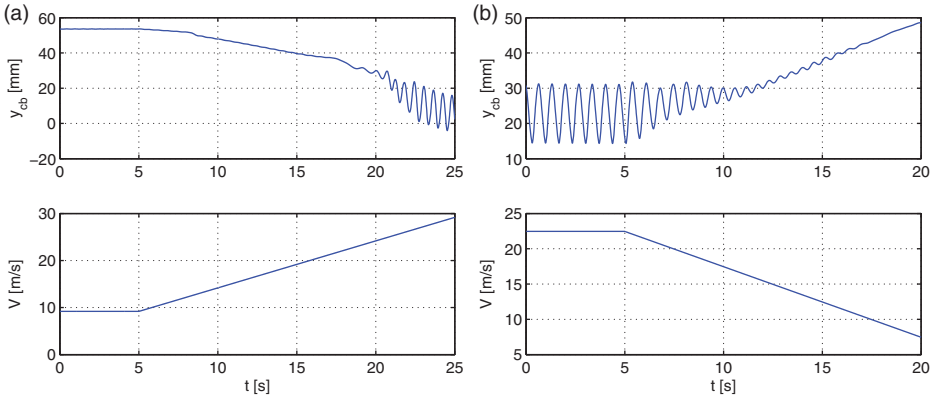

Figure 5. Analysis of the single wagon. Lateral displacement of the carbody using the ramping method, curve radius $R = 300$ m. Left: simulation with increasing speed. Right: simulation with decreasing speed.

The largest oscillation amplitude occurs for both the carbody and trailing wheelset for curve radii in the range of 300–500 m. In order to investigate in further detail, the behaviour of the wagon in this curving condition, the ramping method is applied. Therefore, two additional time-domain simulations are performed for curve radius $R = 300$ m, varying linearly the vehicle speed with time. In one simulation (cf. Figure 5 left), the speed is initially set to the minimum value of 10 m/s and, after the train has reached a steady-state condition in full curve, it is increased up to 30 m/s. In the second one, the speed is initially set to the maximum value of 22 m/s (corresponding to an n.c.l.a. of 0.8 m/s^2) and is then decreased linearly with time until it reaches 8 m/s. The speed increase/decrease is applied with a rate of ± 1 m/s^2. For the sake of brevity, only the results of the carbody lateral displacement are shown.

In the simulation with increasing speed (Figure 5 left), the carbody starts from a stationary position. The corresponding lateral displacement of 55 mm approximately is measured from the track centreline at the longitudinal position of the carbody centre of mass, and is directed towards the curve centre due to the fact that the carbody centreline is approximately lying as a chord of the circumference representing the projection of the track centreline in the horizontal plane. Increasing the speed, the carbody moves outwards (i.e. the lateral displacement decreases), due to the increased centrifugal force and starts to show an oscillatory motion when the speed is approximately equal to 22 m/s. In the simulation with decreasing speed (Figure 5 right) the carbody starts from a steady-state periodic motion; when the speed is decreased the amplitude of the oscillation also decreases but a stationary solution is not reached until the speed is reduced to 12 m/s approximately.

Taking into account that the ramping method leads to an overestimate or an underestimate of the bifurcation speed depending on whether the speed is increased or decreased, it is possible to state that the periodic solution is created by means of a tangent bifurcation, whereas the stationary solution loses its stability due to a Hopf subcritical bifurcation. In the range between approximately 12 and 22 m/s two attractors coexist. This information can be summarised in the bifurcation diagram shown in Figure 6, where all the solutions are plotted as a function of the speed. The stable branches are plotted in continuous line, whereas the unstable branches are represented by means of a dashed line.

Simulations by means of the ramping method are performed also for a larger curve radius ($R = 1000$ m), cf. Figure 7, and different bifurcations are observed. Starting form an initial speed of 20.6 m/s and increasing the speed (Figure 7(a)), a simple periodic solution is observed at speeds above 42 m/s. Decreasing the speed from 41.9 m/s (Figure 7(b)), the solution jumps from the single periodic to a multi-periodic attractor at the speed of 32 m/s. Further decreasing

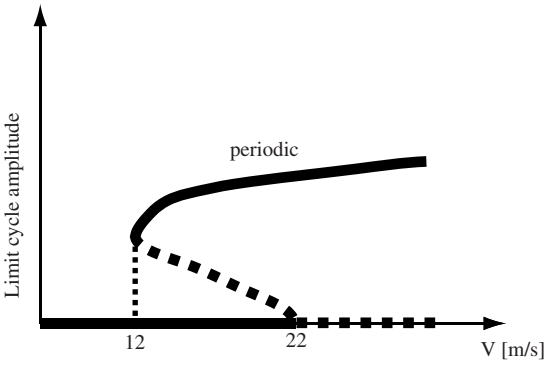

Figure 6. Analysis of the single wagon. Bifurcation diagram, curve radius $R = 300$ m.

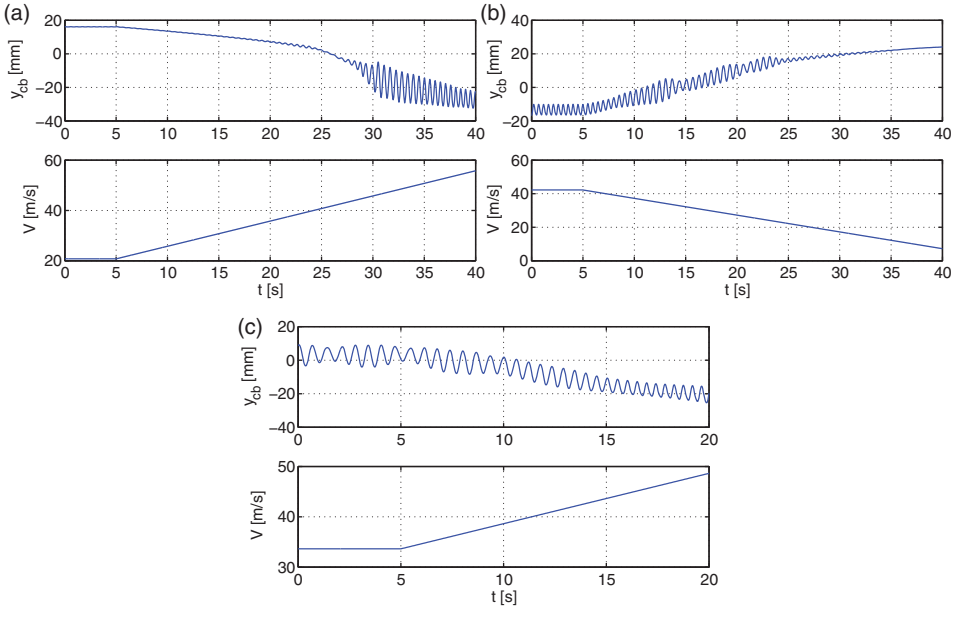

Figure 7. Analysis of the single wagon. Lateral displacement of the carbody using the ramping method, curve radius $R = 1000$ m. (a) Simulation with increasing speed from 20.6 m/s, (b) simulation with decreasing speed from 41.9 m/s and (c) simulation with increasing speed from 33.6 m/s.

the speed, the stationary solution is reached again at 14 m/s. A third simulation was performed using the ramping method with increasing speed starting from the multi-periodic solution, to find its domain of existence (Figure 7(c)): the stable branch of the multi-periodic attractor is found up to approximately 41 m/s.

Figure 8 summarises the bifurcation diagram found for $R = 1000$ m. First a tangent bifurcation creates the multi periodic attractor, further increasing the speed another tangent bifurcation is observed creating the periodic attractor. Then, the stationary solution loses its stability in a Hopf subcritical bifurcation, and, finally, the multi-periodic attractor loses its stability in another Hopf subcritical bifurcation. In the range between 32 and 41 m/s three attractors coexist.

Looking at the results obtained for curve radius $R = 300$ and $R = 1000$ m, it is observed that periodic attractors exist at lower speeds for the curve with shorter radius compared with

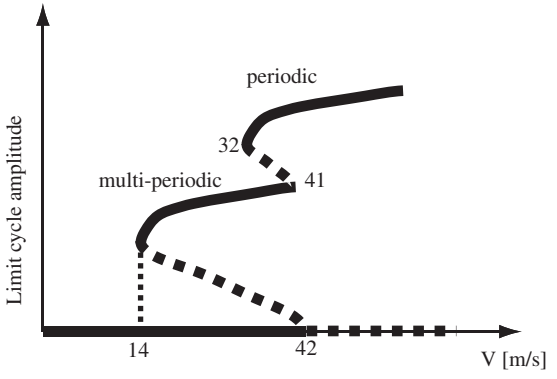

Figure 8. Analysis of the single wagon. Bifurcation diagram, curve radius $R = 1000$ m.

the larger radius curve. This happens because when the wagon negotiates a short radius curve the effective conicity experienced by the leading wheelset is generally higher compared with a larger radius curve, allowing larger amplitudes of motion to appear.

5. Results for a composition of wagons

Aim of this section is to investigate the running dynamics of an assembly of wagons, considering the interaction forces exchanged by the wagons through the buffers and the hook and chain couplers.

In order to keep within reasonable limits the complexity of the overall simulation model, a composition of three wagons is considered: the first one is not representative of any wagon in a real train set, as in a real condition the leading vehicle would be a locomotive, but is used here to reproduce appropriate boundary conditions on the central wagon in the model, which can be regarded as representing any wagon except the last one in the actual train composition. Finally, the third wagon in the model represents the last wagon in a real train set, in case no trailing locomotives are present.

In the same way as described in Section 4, the procedure used to analyse the nonlinear behaviour of the composition of wagons is based on time domain simulations performed considering different combinations of curve radius and train speed. In all simulations, the track cant in full curve corresponds to 150 mm super-elevation of the outer rail. The results presented in this section were obtained for the same Hbbills freight wagons in tare condition already considered in Section 4, whose main parameters are shown in Table 2. The parameters of the buffers and coupler are reported in Table 3.

Table 3. Parameters of the buffer and coupler models.

k_0 (N/m)	k_1 (N/m^2)	k_2 (N/m^3)	k_3 (N/m^4)	k_4 (N/m^5)	r_0 (Ns/m)	r_1 (Ns/m^2)
Buffers						
2.09e6	6.64e7	−2.72e9	5.94e10	−2.03e11	/	2.07e6
Traction gear						
2.93e3	−2.14e2	6.98	−8.15e2	3.35e4	9.24e3	/

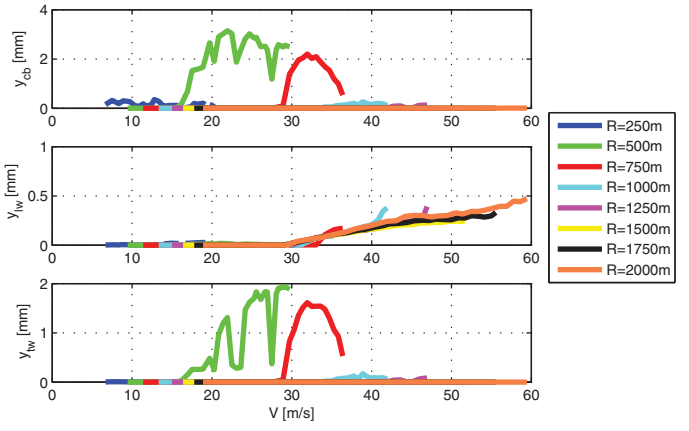

Figure 9. Analysis of the composition of wagons. Map of the lateral oscillation amplitude for the central wagon.

5.1. *Results for the central wagon*

The lateral oscillation amplitude A_{y_i} of the carbody and wheelsets in the central wagon is shown in Figure 9 as function of the vehicle speed for different curve radii. Like in the case of the single wagon analysed in Section 4, the lateral oscillations of the leading wheelset are very small, especially for small radius curves, because of the flange contact of the outer wheel with the rail. As far as the carbody and the trailing wheelset are concerned, oscillatory motion is only observed for curve radii between 300 and 800 m, and for relatively large values of the vehicle speed. In all other cases, both the carbody and trailing wheelset settle on a stationary solution without oscillations. The amplitude of the periodic solution obtained for curve radii between 300 and 800 m is much smaller than in the case of the single wagon, and never exceeds 3 mm. It is, therefore, possible to state that the effect of the buffers and of the draw gear is very important and tends to reduce the lateral oscillations of the wagon up to the point of totally inhibiting lateral oscillations for some combination of curve radius and speed. This can be explained by considering that the coupling system works as a constraint between the wagons, increasing the overall generalized stiffness of the wagon. Since the UIC standard suspension is a relatively soft suspension device, the change in the stiffness of the system provided by the buffers and couplers is substantial, and leads to a completely different dynamic behaviour of the central wagon in a curve.

5.2. *Results for the trailing wagon*

The last wagon in the model is affected by non-symmetric boundary conditions consisting of the interaction with another vehicle only on the front side. Furthermore, because of track curvature the forces generated in the two trailing buffers are unequal, and normally only the inner buffer is in contact. As a result, the force generated in this buffer produces a steering moment on the carbody that strongly affects the dynamics of the wagon, as discussed below.

In Figure 10, the amplitude of the lateral oscillations as function of speed and curve radius is shown for the carbody and wheelsets of the wagon. It is observed that, apart from very small oscillations not exceeding 0.3 mm taking place for small curve radii, the carbody settles always on the stationary solution, without showing any periodic motion. A similar behaviour is observed for the trailing wheelset, which only shows oscillations of even smaller amplitude in limited speed ranges and only for small curve radii. The behaviour of the leading wheelset is otherwise similar to the cases of the single wagon and of the central wagon in the wagon

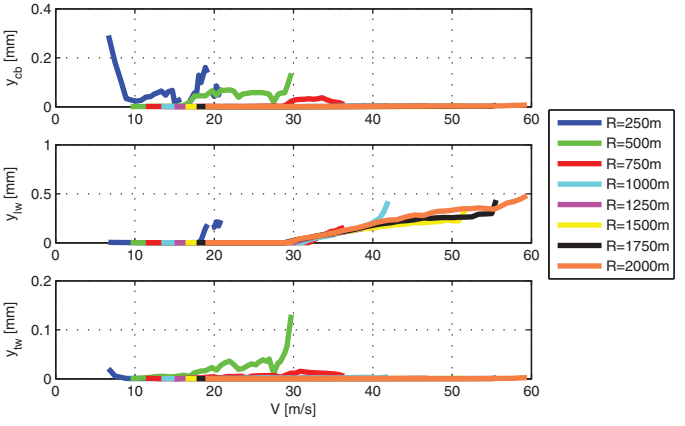

Figure 10. Analysis of the composition of wagons. Map of the lateral oscillation amplitude for the trailing wagon.

assembly. Also for this body, the amplitude of oscillations is small, but occurs for large curve radius and high speed.

In conclusion, it can be stated that the yaw moment due to the forces generated by the coupling system at the trailing side of the vehicle almost suppresses any periodic motion having significant amplitude.

6. Conclusions

In this paper, a mathematical model was introduced to study the running dynamics of a single 2-axle freight wagon and of an assembly of wagons of the same type. The model was used to investigate the running properties and to identify the stationary and periodic solutions for the motion of these wagons in a curve. The model accounts for nonsmooth effects introduced by the dry friction forces acting in the suspensions and by wheel–rail contact forces. When an assembly of wagons is considered, the model additionally accounts for the forces due to the coupling elements, introducing further nonlinear and nonsmooth effects in the analysis.

In the study, wagon-type Hbbills 311 was considered and for the sake of brevity the analysis is confined to the case of the vehicle in tare condition. Wheel and rail were assumed to be shaped according to the ORE S1002 and UIC60 1:20 profiles, respectively.

As far as the running dynamics of the single wagon is concerned, the results obtained show the presence of large periodic oscillations when narrow curves are negotiated at relatively high speeds which nevertheless lie in the range of the commercial operating speed for this type of wagon. Under these running conditions, both the carbody and the trailing wheelset settle into a periodic attractor with large amplitude. Results show that the periodic attractor is generated by a tangent bifurcation and the stationary solution loses its stability in a subcritical Hopf bifurcation.

The analysis performed on a three-wagon assembly, also in tare condition, showed that the effect of the coupling forces on the dynamics of 2-axle freight wagons is very important. In particular, for the central wagon, the lateral oscillation amplitudes are significantly reduced for both the carbody and the trailing wheelset, but periodic solutions having non-negligible amplitude in the range of 2–3 mm are still found for small radius curves negotiated at relatively high speed. On the other hand, for the trailing wagon in the assembly, practically no oscillation was observed. The difference between this wagon and the central one is mainly due to a yaw moment generated by the buffer force on the leading end of the vehicle, which in the case of

the central wagon is not present due to the symmetrical effect of the buffer force acting on the trailing end.

In summary, the results presented show that the running performances of a 2-axle freight wagon in a curve can be considered as not fully satisfactory on account of large oscillations which may arise for some combinations of curve radius and running speed, although these oscillations are quite effectively mitigated by the effect of the interaction forces exchanged by the wagon with the neighbouring vehicles. The reason for this unsatisfactory behaviour lies in the combined effect of the soft lateral suspension provided by the UIC link and the low conicity of the wheel–rail profiles considered in this study. The relatively poor dynamic behaviour of the 2-axle freight wagons may lead to accelerated wear of the wheels and rolling contact fatigue damage in the wheels and rails; these phenomena could be investigated using the simulation model developed in this study and appropriate wear and damage models.

The analysis of other wheel–rail profile cases, namely the ORE S1002 and UIC inclined in 1:40 and worn profiles is a main topic envisaged for future development of this work, as well as the study of the transient behaviour of the wagons when the effect of random disturbances, such as track irregularities, is taken into account.

References

[1] Bruni S, Vinolas J, Berg M, Polach O, Stichel S. Modelling of suspension components in a rail vehicle dynamics context. Vehicle System Dynamics. 2011;49(7):1021–1072.

[2] Awrejcewicz J, Lamarque C-H. Bifurcation and chaos in nonsmooth mechanical systems. World scientific series on nonlinear science: series A Vol. 45. Singapore: World Scientific; 2003.

[3] Di Bernardo M, Budd CJ, Champneys AR, Kowalczyk P, Nordmark AB, Olivar Tost G, Piiroinen PT. Bifurcations in nonsmooth dynamical systems. SIAM Rev. 2008;50(4):629–701.

[4] Leine RI, Nijmeijer H. Dynamics and bifurcations of non–smooth mechanical systems. Berlin Heidelberg New York: Springer-Verlag; 2004.

[5] Kunze M. Non–smooth dynamical systems. Berlin Heidelberg New York: Springer; 2000.

[6] True H. On the theory of nonlinear dynamics and its applications in vehicle system dynamics. Veh Syst Dyn. 1999;31(5–6):393–421.

[7] Fancher PS, Ervin RD, MacAdam CC, Winkler CB. Measurement and representation of the mechanical properties of truck leaf springs. SAE Trans; 1980; Warrendale, PA.

[8] Cebon D. Handbook of vehicle–road interaction. Lisse (Netherlands): Swets & Zeitlinger; 1999.

[9] Piotrowski J. Model of the UIC link suspension for freight wagons. Arch Appl Mech. 2003;73:517–532.

[10] Piotrowski J. A new measurement method for determination of mechanical characteristics of pendulous systems with friction. 3rd international conference “Modelling and simulation of friction phenomena in physical and technical systems”; Warsaw University of Technology; 2004 May 31; Warsaw, Poland.

[11] Grzelak A. Influence of wear of elements of UIC link suspension on ride dynamics of freight wagon on a straight track [PhD thesis]. Institute of Vehicles, Warsaw University of Technology; 2006.

[12] Jönsson P-A. Modelling and laboratory investigations on freight wagon link suspensions, with respect to vehicle–track dynamic interaction [PhD thesis]. Sweden: KTH Aeronautical and Vehicle Engineering, Royal Institute of Technology (KTH) 2004.

[13] Stichel S. How to improve the running behaviour of freight wagons with UIC–link suspension. Veh Syst Dyn Suppl. 1999;33:394–405.

[14] Stichel S. Limit cycle behaviour and chaotic motions of 2–axle freight wagons with friction damping. Multibody Syst Dyn. 2002;8:243–255.

[15] Stichel S. The influence of underframe structural flexibility on the hunting behaviour of a freightwagon. Paper presented at: 7th Internation Conference on Computers in Railways;2000; Bologna, Italy. p. 725–736.

[16] Hoffmann M. Dynamics of European 2-axle freight wagons [Ph.D. thesis]. IMM Department of Informatics and Mathematical Modelling, Technical University of Denmark (DTU); 2006.

[17] True H. Dynamics of railway vehicles and rail/wheel contact. In: Schiehlen W, editor. Dynamical analysis of vehicle systems. Wien New York: Springer; 2009. p. 75–128.

[18] Bruni S, Collina A, Diana G, Vanolo P. Lateral dynamics of a railway vehicle in tangent track and curve: tests and simulation. Veh Syst Dyn Suppl. 1999;33:464–477.

[19] Braghin F, Bruni S, Diana G. Experimental and numerical investigation on the derailment of a railway wheelset with solid axle. Veh Syst Dyn. 2006;44(4):305–325.

[20] Kik W, Moelle D, Bogo C, Ferrarotti G. The Manchester benchmarksADAMS/rail – MEDYNA statement of methods. Veh Syst Dyn Suppl. 1999;31:49–65.

[21] Belforte P, Cheli F, Diana G, Melzi S. Numerical and experimental approach for the evaluation of severe longitudinal dynamics of heavy freight trains. Veh Syst Dyn Suppl. 2008;46:937–955.
[22] Cheli F, Melzi S. Experimental characterization and modelling of a side buffer for freight trains.Proc Inst Mech Eng, Part F: J Rail Rapid Transit. 2010;224(6):535–546.
[23] Cantone L, Crescentini E, Verzicco R, Vullo V. A numerical model for the analysis of unsteady train braking and releasing manoeuvres. Proc. IMechE, Part F: J Rail Rapid Transit. 2009;223(3):305–317.
[24] Cheli F, Melzi S, Di Gialleonardo E. Numerical analysis of curving performances of low flatcar wagons. Int J Heavy Veh Syst. 2011;18(2):195–213.
[25] Belforte P, Cheli F, Diana G, Facchinetti A, Melzi S. A numerical model for the analysis of heavy freight trains dynamics with respect to running safety. Multibody Dynamics 2007-ECCOMAS Thematic Conference, Politecnico di Milano, Milan, Italy; 2007.